Physics – Uspekhi **41** (2) 167 – 189 (1998)

CONFERENCES AND SYMPOSIA

PACS numbers: **05.50.+q**, 73.20.Dx

Mesoscopic and strongly correlated electron systems "Chernogolovka 97"

4. Quasi-1D systems, networks and arrays

The fourth session of the conference included the following presentations:

(1) **Noat Y, Bouchiat H, Reulet B** (Universite Paris-Sud, Orsay, France), **Mailly D** (Bagneux, France) "Electromagnetic responses of isolated quantum rings and dots: from discrete to continuous spectrum";

(2) **van der Zant H S J, Mantel O C, Rutten P W F, Dekker C** (Delft University of Technology, Delft, the Netherlands) "Electrical transport through micro-fabricated charge-density-wave structures";

(3) **Oreg Y** (The Weizmann Institute of Science, Israel), **Finkel'stein A M** (The Weizmann Institute of Science, Israel; Landau Institute for Theoretical Physics, RAS, Chernogolovka, Russia) "Flow diagram for impurity scattering in Tomonaga – Luttinger liquids";

(4) **Devoret M** (CEA – Saclay, France) "Shot noise in mesoscopic metallic resistors";

(5) **Pothier H, Esteve D** (CEA – Saclay, France) "Direct observation of energy exchange between quasiparticles in mesoscopic wires";

(6) **Hansen W, Schmerek D, Steinebach C** (Institut für Angewandte Physik, Zentrum für Mikrostrukturforschung, Universität Hamburg, Germany) "Ground states in one-dimensional electron systems";

(7) **Gorelik L, Kulinich S** (Chalmers University of Technology, and Goteborg University, Goteborg, Sweden; B Verkin Institute for Low Temperature Physics and Engineering, Khar'kov, Ukraine), **Galperin Yu** (University of Oslo, Oslo, Norway, and A F Ioffe Institute, St. Petersburg, Russia), **Shekhter R I, Jonson M** (Chalmers University of Technology and Goteborg University, Goteborg, Sweden) "Pumping of energy into a mesoscopic ring. Exactly solvable model";

(8) **Kitaev A** (Landau Institute for Theoretical Physics, RAS, Chernogolovka, Russia) "Quantum computation: physical requirements";

(9) **Martinoli P, Eichenberger A L, Meyer R** (Universite de Neuchatel, Switzerland), **Korshunov S E** (Landau Institute for Theoretical Physics, RAS, Chernogolovka, Russia) "Crossover phenomena in disordered and fractal Josephson junction arrays";

(10) **Ustinov A et al.** (University of Erlangen – Nuremberg, Germany, and Institute of Solid State Physics, RAS, Chernogolovka, Russia) "Cherenkov radiation of Josephson vortices";

(11) **Pascaud M, Montambaux G** (Laboratoire de Physique des Solides, associe au CNRS Universite Paris-Sud, Orsay, France) "Interference effects in mesoscopic disordered rings and wires";

(12) **Molenkamp L** (Physikalisches Institut, RWTH – Aachen, Germany) "Novel transport effects in quantum-device circuits";

(13) **Chaplik A V, Govorov A O** (Institute of Semiconductor Physics, Novosibirsk, Russia) "Collective modes and quantum fluctuations in an array of spontaneously polarized quantum dots";

(14) **Gershenson M E, Khavin Yu B** (Rutgers University, USA), **Bogdanov A L** (Lund University, Sweden) "Electrons in quasi-one-dimensional conductors: from high-temperature diffusion to low-temperature hopping".

Papers 2, 3, 6, 7, 11 and 14 are published below. For papers 1 and 8 see the e-prints: 1 — cond-mat/9711171; 8 — quant-ph/9707021.

Uspekhi Fizicheskikh Nauk **168** (2) 179 – 203 (1998)
Translated by M V Magnitskaya;
edited by M V Feĭgel'man and L V Semenova

Electrical transport through micro-fabricated charge-density-wave structures

H S J van der Zant, O C Mantel,
P W F Rutten, C Dekker

1. Introduction

Electrical conductors with a chain-like structure may exhibit a phase transition to a collective ground state with charge-density waves (CDWs) [1]. The appearance of a CDW state is connected to the Peierls instability [2]: at low temperatures the uniform distribution of conduction electrons of a one-dimensional (1D) conductor is unstable due to their coupling to phonon modes. The lattice of atoms is distorted and the electrons condense into a ground state with a periodic modulation of the charge density. This Peierls phase transition has been observed in a variety of CDW materials such as $NbSe_3$, TaS_3 and the blue bronzes $A_{0.30}MoO_3$ with A = K, Rb, Cs [3, 4].

In equilibrium, the CDW is pinned to impurities and conduction is only possible by quasi-particles that are excited above the energy gap $\Delta(T)$. For the blue bronzes, all electrons are condensed in the CDW state, so that at low temperatures they act like semi-conductors. When a moderate electric field is applied, however, the CDWs can slide collectively, resulting in highly nonlinear current-voltage characteristics. Most dynamic CDW properties can qualitatively be understood

within the Fukuyama – Lee – Rice (FLR) model [5]. In this model, the CDW is viewed as an elastic medium that interacts with impurities. Within the FLR phase-coherence length the elastic medium is undistorted by the impurities. To date, a study of CDW dynamics on samples with all dimensions smaller than the phase-coherence lengths has not been performed.

New quantum phenomena are expected to occur in phase-coherent CDW transport. A recent experiment [6] reports on such a new effect. An oscillating magnetoresistance with period $h/2e$ was observed in irradiated $NbSe_3$ crystals with columnar defects with a diameter of 15 nm. These oscillations are the response of ensemble averaging over about 10^6 rings. A possible explanation is that if a substantial part of the sample is phase coherent the oscillations are Aharonov – Bohm oscillations. Rejaei and Visscher [7] have suggested an alternative explanation for the observed resistance oscillations. They propose that the magnetic flux modulates the threshold field and that the periodicity of $\Phi_0/2$ results from ensemble averaging over random scattering phases of the rings.

On a microscopic level, the CDW transition can be interpreted as a Bose condensation of electron – hole pairs, analogous to the condensation of Cooper pairs into the superconducting state. Collective CDW transport displays many similarities with transport in superconductors, with the role of current and voltage reversed. For example, a current – frequency relation exists for the collective CDW current, analogous to the ac Josephson relation between voltage and frequency in superconductors. The analogy with superconductors has led to speculations about the possible occurrence of Andreev-like reflection at a normal metal – CDW interface. Current conservation requires that in the N – CDW case, the electron is retro-reflected as an electron instead of a hole. Recent tunneling experiments [8] at a Cu – $Rb_{0.30}MoO_3$ interface have been interpreted in this way. A theoretical study [9] on the other hand, showed that retro-reflection can not occur since the electron – hole pair in the condensate carries a momentum of $2k_F$. Instead, electrons can be Bragg reflected from the CDW. The precise mechanism for conversion of electrons into the CDW condensate is still under debate.

Experiments on CDWs so far have been performed on bulk crystals. Recently, we have reported [10, 11] on thin-film growth of the CDW oxide $Rb_{0.30}MoO_3$. We have developed a process to fabricate (sub)micron CDW structures so that a systematic study of phase-coherent CDW transport is possible. Our thin-film technology not only permits the study of phase-coherent structures, but also of completely new artificial structures. Deposition of CDW materials can be combined with deposition of either normal metals, superconductors or insulators to form multi-layers or to fabricate CDW junctions. Such mesoscopic structures open up a new line of research in the field of CDWs.

2. Thin-film growth of $Rb_{0.30}MoO_3$

We use pulsed-laser deposition for the fabrication of thin $Rb_{0.30}MoO_3$ films [10, 11]. The set-up consists of a laser and a vacuum chamber. The laser hits a polycrystalline $Rb_{0.30}MoO_3$ target in the vacuum chamber to which some oxygen is applied. A substrate, mounted on a heater block, is situated opposite to the target. $Rb_{0.30}MoO_3$ films can be made at oxygen pressures ranging from 100 – 175 mTorr and substrate temperatures from 350 to 450 – 500 °C. The upper boundary for the temperature depends on the deposition rate which can be changed by varying the laser power, the repetition rate of the laser and the target – substrate distance. Typical deposition rates and film thicknesses are 0.05 – 1.5 nm s^{-1} and 100 – 1000 nm, respectively.

All films are granular with most grains oriented such that the CDW-axis (*b*-axis) is parallel to the substrate surface. Grain size increases with increasing substrate temperature and decreasing deposition rate. Surface corrugation increases with increasing deposition temperature and is substantial (of the order of the film thickness for films grown at temperatures 440 – 500 °C).

On $Al_2O_3(012)$ substrates, disk-like grains of submicron sizes are formed at substrate temperatures of 375 – 400 °C. At higher deposition temperatures, the grains have a more elongated shape. At 470 °C these grains are about 5 μm long. Grains are randomly distributed on the substrate surface. X-ray analysis demonstrates that the *b*-axis is also randomly oriented within the surface plane.

On $SrTiO_3$ substrates, we find hetero-epitaxial growth. On $SrTiO_3(100)$, elongated grains are oriented in two perpendicular directions along the principal axes of the substrate surface lattice. The *b*-axis runs parallel to the long axes of these grains. Depending on the deposition rate, films grown at 375 °C have grains with sizes of 0.1 by 0.5 μm^2 to 0.3 by 1 μm^2. Films grown at 440 °C have larger grain sizes ranging from 0.2 by 1 μm^2 to 1 by 5 μm^2. By using $SrTiO_3(510)$ substrates, the majority of the grains can be oriented in one direction, albeit only for growth at 375 °C. The submicron grains have an elongated shape and their long axis runs along the [001]-axis of the $SrTiO_3(510)$ substrate.

3. Photolithography on $Rb_{0.30}MoO_3$ thin films

Standard photolithography is done with SR1813, a positive resist sensitive to near-UV light. When spin coated at a speed of 5000 rpm, this resist is 1.3 μm thick in the middle of the samples. After applying the resist, the sample is baked at 90 °C for 30 minutes. Exposures are made through a glass mask with a Karl Susz aligner. The resist is then developed in a water-based AZ-developer for 45 – 75 s. Since our substrates are small, typically 5 by 5 mm^2, a substantial part near the sample edges has a thicker resist layer. Before starting, this thicker resist layer near the edges is removed in a separate process step with a centered 4 by 4 mm^2 mask. Etching is done by means of dry argon ion milling in a home-made set-up with a Kaufmann source. During etching, the sample is water cooled. Blue bronze is typically etched at a rate of 300 – 450 nm per hour. This rate is about a factor 5 – 10 slower than the etch rate of evaporated gold films.

Fabrication of a sample consists of two process steps: first the $Rb_{0.30}MoO_3$ lines are etched into the film (Fig. 1 a – d) and secondly the metal contacts are defined on top of the $Rb_{0.30}MoO_3$ lines (Fig. 1 e – g). We found that if the $Rb_{0.30}MoO_3$ films are in direct contact to the developer for more than 30 s, parts of the $Rb_{0.30}MoO_3$ film peel off from the substrate. To avoid contact with the developer, $Rb_{0.30}MoO_3$ films have to be separated by a buffer layer from the resist during the first process step. As a buffer layer we use 200 nm Au on top of 15 nm Cu. Structures are then obtained by etching first through the Cu/Au sandwich and subsequently through the blue bronze film (see also Fig. 1). Etching is stopped when the resist as well as the Cu/Au is removed on those places where $Rb_{0.30}MoO_3$ remains. For a $Rb_{0.30}MoO_3$

film of 450 nm thick, etching of the resist takes about as much time as the etching of $Rb_{0.30}MoO_3$, so that a $Rb_{0.30}MoO_3$ structure on a cleaned substrate is obtained.

For the definition of the contact pads a lift-off mask can not be used because in this case the $Rb_{0.30}MoO_3$ will be in direct contact with the developer. Instead, we use an etch mask consisting of resist on top of a Cu/Au sandwich (see Fig. 1 e – g). Contacts between the $Rb_{0.30}MoO_3$ wire and the Cu/Au metal layer are now formed at those places where the resist has not been developed. Since etching of the Cu/Au layer only takes 5 – 10 minutes, resist still remains on the Cu/Au contact pads. This remaining resist is removed (the resist strip) in warm acetone for 15 minutes. A photograph of a completed sample is shown in Fig. 2. Finally, bond wires are then connected to the Au layer.

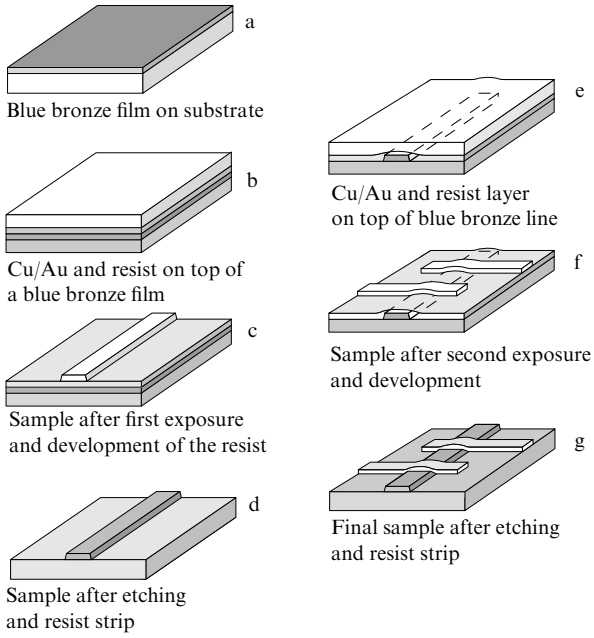

Figure 1. Fabrication process for photolithographic patterning of a wire in a $Rb_{0.30}MoO_3$ film (a – d) and of contact pads on top of it (e – g).

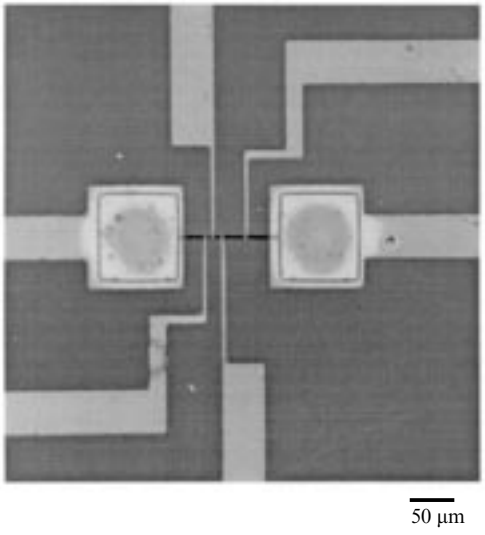

Figure 2. Photograph of a 100 μm long, 2.5 μm wide and 0.3 μm high $Rb_{0.30}MoO_3$ wire. The gold squares at both ends are used for current injection. Voltage probes are spaced 5, 10 and 25 μm apart.

A general problem during the processing is the bad adhesion of $Rb_{0.30}MoO_3$ to the substrate. The adhesion of the normal metal to the $Rb_{0.30}MoO_3$ film is generally also poor. We have tried several ways and combinations of metals to overcome this latter problem. Our best results were obtained using a sandwich of 15 – 30 nm Cu covered with 150 – 300 nm Au. The contact resistance between Cu and the $Rb_{0.30}MoO_3$ films varies from wire to wire. It can be much smaller than or of the order of the $Rb_{0.30}MoO_3$ sheet resistance at all temperatures.

4. Electrical transport of $Rb_{0.30}MoO_3$ wires

4.1 Quasi-particle transport

Four-terminal measurements have been performed on 9 different wires made of $Rb_{0.30}MoO_3$ films grown with different substrates, temperatures and deposition rates. Figure 3 shows the quasi-particle resistivity of one such wire measured as a function of temperature. This wire was made in a film deposited at a high temperature of 470 °C. The wire resistance (R) is measured with standard lock-in techniques. The data clearly show the expected increase of the resistance below the Peierls temperature T_P of 178 K. This value is close to the bulk value of 182 K. In the inset, we plot $d(\ln R)/dT$ as a function of temperature which is a common way to visualize the Peierls phase transition. In bulk crystals a clear dip in $d(\ln R)/dT$ is observed at T_P. Our measurement also shows this dip at T_P although less pronounced than in crystals.

The dashed line in Fig. 3 is an exponential temperature dependence with a gap according to the BCS model: $R \propto \exp[\Delta(T)/k_B T]$. The fit parameter $\Delta(0)/k_B$ is 480 K for this wire. The bulk value of $\Delta(0)/k_B$ is 520 K †. We have found a systematic decrease of $\Delta(0)$ as a function of grain size. For samples made of films grown at 375 °C, the zero-temperature gap is found to be only 400 K. A reduction of $\Delta(0)$ due to finite-size effects may be expected but at this moment the precise mechanism is still unclear. However, to explain our data, the mechanism should predict a gap reduction at length scales of the order of a few hundred nanometers i.e., about two orders of magnitude larger than the CDW BCS-coherence length of 1 nm [1].

At room temperature, the resistivity of the wire in Fig. 3 is 2.4 mΩ cm. This is the lowest value we have obtained so far. For other wires, the room-temperature resistivity ranges from 7 to 500 mΩ cm. The value of 2.4 mΩ cm is only a factor two higher than the value for the bulk-crystal resistivity along the CDW axis [12, 13]. In the direction perpendicular to the CDW axis (but still in-plane), the resistivity is about a factor 20 – 80 higher [12, 13]. Thus, a grain oriented with its *b*-axis perpendicular to the current direction would have a resistivity of 20 – 80 mΩ cm. In wires with resistivities higher than 20 – 80 mΩ cm grain boundaries must play a dominant role. For wires with resistivities between 1 and 20 – 80 mΩ cm, the anisotropy of $Rb_{0.30}MoO_3$ may be dominant, but effects due to grain boundaries can not be excluded.

Starting at room temperature the resistance of a bulk $Rb_{0.30}MoO_3$ crystal initially decreases with decreasing tem-

† We have also measured the temperature dependence of the resistance across a $Rb_{0.30}MoO_3$ crystal. An analysis similar to that presented in this paper yielded a zero-temperature energy gap of 520 K.

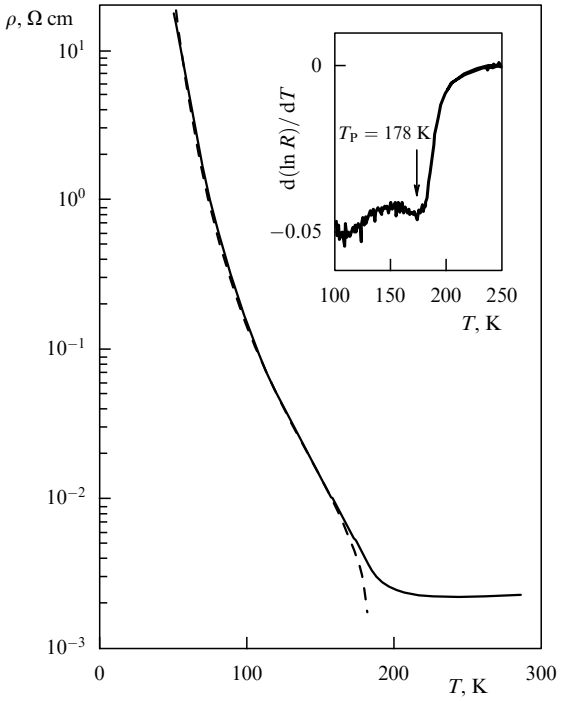

Figure 3. Four-probe resistivity ρ of wire with dimensions 5 by 2.5 by 0.3 μm^3. The wire is made in a film grown on an $Al_2O_3(012)$ substrate at a temperature of 470 °C. Inset: the same data plotted as $d(\ln R)/dT$ versus T, illustrating the behavior near the Peierls transition.

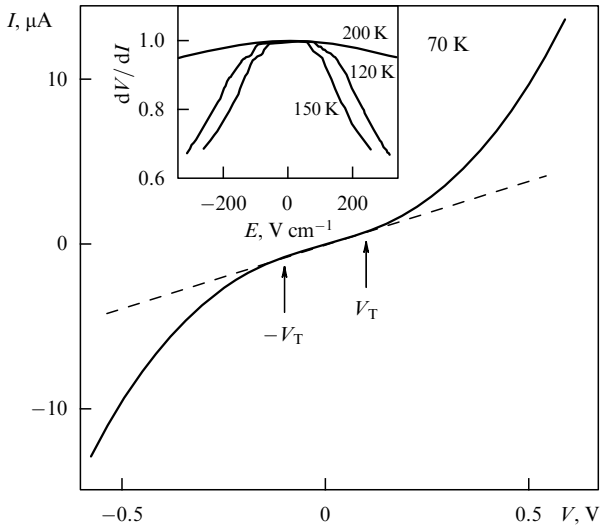

Figure 4. Four-terminal current-voltage characteristics of the wire whose temperature dependence on the linear resistivity was shown in Fig. 3. The dashed line shows the quasi-particle resistance. Near a threshold voltage of $V_T = 0.1$ V, $I-V$ becomes nonlinear. Inset: the normalized differential resistance dV/dI vs electric field for three different temperatures.

perature. In Figure 3 we observe a similar decrease of the resistance in our $Rb_{0.30}MoO_3$ wire with a temperature coefficient that is in agreement with reported values for bulk crystals [14]. For most other wires we observe, however, a slight increase of the resistance as the temperature is lowered. An exponential dependence of the resistance on temperature can be fitted to this insulating-like behavior. The corresponding energy barrier in this thermally activated process ranges from 250 K for films grown at low temperatures to about 50–100 K for films grown at higher temperatures. The thermally activated behavior above the Peierls transition is likely due to the granular nature of our films.

The low-bias transport properties of the wire of Fig. 3 are clearly not dominated by grain boundaries. In fact, its low-bias properties resemble those of bulk crystals. Values of the energy gap, the Peierls temperature and the room-temperature resistivity all are close to reported values for bulk crystals. In addition, at room temperature metallic-like behavior is observed as expected for $Rb_{0.30}MoO_3$. The high-bias properties of this wire will be discussed in the next subsection.

4.2 Sliding CDWs

We have measured the current-voltage characteristics at various temperatures. Simultaneously, we have recorded the differential resistance (dV/dI) with a lock-in technique. The ac amplitude was 2.5% of the full dc current-scale. As illustrated in Fig. 4, the current-voltage characteristic measured at 70 K is clearly nonlinear. For low-bias voltages, the $I-V$ curve is linear (dashed line). Near a threshold voltage of 0.1 V a smooth transition to a nonlinear region sets in.

In the inset of Fig. 4 we have plotted the normalized differential resistance vs voltage. At 200 K, i.e., above the Peierls temperature of 178 K, the differential resistance only decreases by a few percent for fields up to 300 V cm^{-1}. (At room temperature (not shown), the differential resistance shows a slight (0.5%) increase with increasing field). Just below the Peierls temperature, the differential resistance behaves dramatically differently, consistent with the expected dynamics associated with sliding CDWs. A sharp decrease of dI/dV is visible which appears at 60 V cm^{-1}. A step-like structure is seen which we attribute to depinning of the CDWs in two different grains between our voltage probes. When decreasing the temperature to 120 K the threshold field increases. Below 100 K, E_T remains almost constant but the threshold itself becomes less pronounced.

Our threshold fields are at least one order of magnitude higher than the highest reported in the literature. Measurements [15–17] on crystals have shown a trend of increasing E_T as the cross-sections get smaller. For example, a bulk $Rb_{0.30}MoO_3$ sample with a cross-section of 90 nm by 110 μm has shown a threshold field of 4 V cm^{-1} [17]. At this moment we do not have an explanation for the high threshold fields observed in our wires. The other wires with higher resistivities show threshold fields that are at most a factor 4 higher than those shown in the inset of Fig. 4. We have not observed a correlation between E_T and the resistivity of the wires.

Additional evidence for sliding CDWs is obtained from measuring the noise voltage as a function of the electric field. In the sliding state, $1/f$-like noise arises due to the fact that there are several phase-coherent CDW regions that move with different velocities [9]. This broad-band noise is commonly observed in bulk CDWs. In Figure 5 we compare the noise power spectral densities measured with an SRS spectrum analyzer at 0 V and at 0.3 V across a $Rb_{0.30}MoO_3$ wire. At $V = 0$ V, the CDWs are pinned and the noise level is limited by our measurement equipment. At voltages above the threshold voltage, the noise at low frequencies has increased by many orders of magnitude. The dashed line in Fig. 5, represents a line with slope −1 ($1/f$ noise). In the inset, we plot the rms noise voltage ($S_V(f)$ integrated over the full bandwidth) versus the voltage across the wire. At low voltages the rms noise voltage is almost zero, but near V_T a dramatic

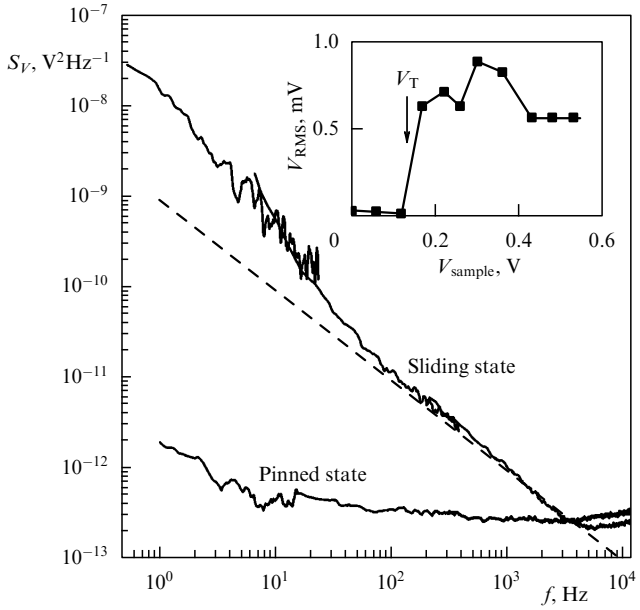

Figure 5. Noise-power spectral density of the output signal measured across an $Rb_{0.30}MoO_3$ wire at $V = 0$ V (pinned state) and at $V = 0.3$ V (sliding state). Inset: the rms noise voltage measured at different voltages.

increase in the noise voltage is observed as expected from CDW dynamics.

5. Conclusions

We have presented four-probe measurements on CDW wire structures with micron-size dimensions. Wires are made in thin films consisting of single-phase $Rb_{0.30}MoO_3$ with a granular structure. The quasi-particle resistance measured as a function of temperature clearly reveals the expected opening of an excitation gap at a Peierls temperature of 180 K. The value of the zero-temperature gap is suppressed for films with the smallest grain sizes. We clearly observe nonlinear current-voltage characteristics, indicative of the sliding of CDWs. The threshold field is much higher than reported on bulk crystals.

Finite-size effects may play a role, but the possibility of CDW depinning from grain boundaries or contact interfaces must also be considered.

Acknowledgments. We wish to acknowledge Hans Mooij, Mark Visscher, Behzad Rejaei, and Gerrit Bauer for discussions, Leo Lander for technical assistance, Jip Steinfort for X-ray analysis, and Chresten Træholt and Henny Zandbergen for TEM work. Research was supported by the Netherlands Foundation for Fundamental Research on Matter (FOM).

References

1. Grüner G *Density Waves in Solids* (Frontiers in physics Vol. 89) (Reading, Mass: Addison – Wesley Pub. Co. 1994)
2. Peierls R E *Quantum Theory of Solids* (Oxford: Clarendon Press, 1955)
3. Monceau P, in *Electronic Properties of Quasi-One-Dimensional Metals* (Ed. by P Monceau) (Dordrecht: Reidel, 1985) Vol. 2.
4. Schlenker C et al., in *Low-Dimensional Properties of Molybdenum Bronzes and Oxides* (Ed C Schlenker) (Dordrecht: Kluwer Academic Publishers, 1989) p. 159 – 257
5. Fukuyama H, Lee P A *Phys. Rev. B* **17** 535 (1978); Lee P A, Rice T M *Phys. Rev. B* **19** 3970 (1979)
6. Latyshev Yu I et al. *Phys. Rev. Lett.* **78** 919 (1997)
7. Visscher M I, Rejaei B *Phys. Rev. Lett.* **79** 4461 (1997)
8. Sinchenko A A et al. *Pis'ma Zh. Eksp. Teor. Fiz.* **64** 259 (1996) [*JETP Lett.* **64** 285 (1996)]
9. Artemenko S N, Remizov S V *Pis'ma Zh. Eksp. Teor. Fiz.* **65** 50 (1997) [*JETP Lett.* **65** 53 (1997)]
10. van der Zant H S J et al. *Appl. Phys. Lett.* **68** 3823 (1996)
11. Mantel O C et al. *Phys. Rev. B* **55** 4817 (1997)
12. Bervas E, Thèse de docteur ingenieur (Université de Grenoble, 1984)
13. Sato M et al. *J. Phys. C* **18** 2603 (1985)
14. Brütting W et al. *Phys. Rev. B* **51** 9533 (1995)
15. Borodin D V, Zaitsev-Zotov S V, Nad' F Ya *Zh. Eksp. Teor. Fiz.* **93** 1394 (1987) [*Sov. Phys. JETP* **66** 793 (1987)]
16. McCarten J et al. *Phys. Rev. Lett.* **63** 2841 (1989)
17. Xue-mei W, Dian-lin Z, Yuheng Z *Phys. Rev. B* **45** 13250 (1992)
18. Bhattacharya S et al. *Phys Rev. Lett.* **54** 2453 (1985)

Flow diagram for impurity scattering in Tomonaga – Luttinger liquids

Y Oreg, A M Finkel'stein

1. Introduction

The electron liquids in quantum wires are usually described in terms of the Tomonaga – Luttinger (TL) model [1]. Edge states in a two-dimensional electron gas, under conditions of the fractional quantum Hall effect, were argued to be TL liquids as well [2]. It is well known that in the TL model with a repulsive electron – electron (e – e) interaction the effective strength of backward scattering by an impurity defect increases with decreasing temperature [3]. For this reason, the description of a single defect in a TL liquids is based on the assumption [4 – 6] that at low temperatures the asymptotic behavior of the system may be described as tunneling between two disconnected semi-infinite TL wires. The effective amplitude of tunneling between the half-wires scales to zero with decreasing temperature, because the tunneling density of states at the ending point of a TL liquid vanishes when the e – e interaction is repulsive. This description corresponds to a scenario in which the effective strength of the impurity increases in the course of the renormalization, so that at the final stage a weak impurity transforms into a strong barrier, and disconnects the TL wire. However, a direct calculation of the tunneling density of states [7] obtained by a mapping of the weak impurity problem onto a Coulomb gas theory, apparently contradicts this intuitive picture. It has been found that at the location of a weak impurity the tunneling density of states is enhanced, rather than vanishing. The scenario in which a weak impurity eventually disconnects a TL wire assumes that no other fixed points intervene in the scaling from the repulsive fixed point of a weakly scattering defect to the attractive fixed point corresponding to a tunneling junction of two half-wires. The contradiction by this scenario of calculations of single particle properties, such as the tunneling density of states [7], and the Fermi edge singularity [8], indicates that maybe this is not the case.

In this work the problem of a single impurity in TL liquids with a repulsive e – e interaction is reinvestigated. We concentrate on the limit when the Fermi wave length is much larger than the defect size. This situation is typical for semiconductors, where the filling of the conduction band is